Exploring the gating mechanisms of aquaporin-3

de Almeida, A.; Martins, A. P.; Mosca, A. F.; Wijma, H.J.; Prista, C.; Soveral, G.; Casini, A.

Published in:
Molecular BioSystems

DOI:
10.1039/c6mb00013d

Publication date:
2016

Molecular BioSystems

PAPER

View Article Online
View Journal | View Issue

Cite this: *Mol. BioSyst.*, 2016, 12, 1564

Received 6th January 2016,
Accepted 2nd March 2016

DOI: 10.1039/c6mb00013d

www.rsc.org/molecularbiosystems

Exploring the gating mechanisms of aquaporin-3: new clues for the design of inhibitors?†

A. de Almeida,‡[a] A. P. Martins,‡[bc] A. F. Mósca,[bc] H. J. Wijma,[d] C. Prista,[e] G. Soveral*[bc] and A. Casini*[af]

The pH gating of human AQP3 and its effects on both water and glycerol permeabilities have been fully characterized for the first time using a human red blood cell model (hRBC). For comparison, the effects of pH on the gating of rat AQP3 have also been characterized in yeast. The obtained results highlight similarities as well as differences between the two isoforms. In addition, we investigated the molecular mechanism of hAQP3 pH gating *in silico*, which may disclose new pathways to AQP regulation by small molecule inhibitors, and therefore may be important for drug development.

Introduction

Aquaporins (AQPs) are transmembrane proteins, assembled in tetramers in membranes, responsible for fluxes of water and glycerol in most organisms.[1] The 13 known mammalian isoforms (AQP0–12) are expressed in various tissues/organs and have different permeabilities, structural features and localization, and can be divided into three main groups: (i) orthodox (also named classical) aquaporins, selective for water permeability (AQPs 0, 1, 2, 4, 5, 6 and 8); (ii) aquaglyceroporins, permeable to water, but also to glycerol and other small solutes (AQPs 3, 7, 9 and 10); (iii) superaquaporins (AQP11–12), intracellular isoforms that have much lower sequence homology with the other aquaporin isoforms.[2] Interestingly a few aquaporins do not fit in only one category; thus for example AQP6 and AQP8 are both classified as classical aquaporins, even though AQP6 is an intracellular isoform, found in vesicles, which has been shown to be a functional pH-sensitive chloride channel, and AQP8 is also permeated by urea, ammonia and hydrogen peroxide.[3–5] Finally, AQP11 has also been reported to be permeated by glycerol.[6]

Due to their numerous roles in physiology, these proteins are essential membrane channels involved in crucial metabolic processes. Much of our understanding of AQP functions in mammalian physiology has come from the relatively recent phenotype analysis of mice lacking one of the AQPs. These studies have confirmed the anticipated involvement of AQPs in the mechanism of urine concentration and glandular fluid secretion, and led to the discovery of unanticipated roles of AQPs in brain water balance, cell migration (angiogenesis, wound healing), neural function (sensory signalling, seizures), epidermis hydration and ocular function.[7] Specifically, the 'aquaglyceroporins' regulate glycerol content in epidermal, fat and other tissues, and appear to be involved in skin hydration, cell proliferation, carcinogenesis and fat metabolism.[7,8]

AQPs can be subjected to regulation *via* different means. For example, some orthodox aquaporins are regulated by post-translational modifications, as phosphorylation,[9–12] as well as gated by sudden osmotic changes and membrane surface tension,[10,13–15] divalent cations[16,17] and pH.[18,19] The orthodox water channels AQP0 (expressed in the lens) and AQP6 (expressed in the intercalated cells of the kidney collecting ducts) are gated by pH and appear to have low permeability at physiological pH, increasing below pH 7 and with a maximum of permeability at about pH 6.5.[3,20]

As far as aquaglyceroporins are concerned, information about gating mechanisms is only available for AQP3, which can be regulated by both pH and divalent cations.[21–23] Interestingly, at variance with AQP0 and AQP6, AQP3 shows an overall maximum of permeability for water and glycerol above pH 6.5, decreasing with lower pH, until complete pore closure at pH 5.[21,22] As AQP0 and AQP6 are both orthodox aquaporins and AQP3 is permeated

[a] *Dept. of Pharmacokinetics, Toxicology and Targeting, Groningen Research Institute of Pharmacy, University of Groningen, A. Deusinglaan 1, 9713 AV Groningen, The Netherlands*
[b] *Research Institute for Medicines (iMed.ULisboa), Faculty of Pharmacy, Universidade de Lisboa, 1649-003 Lisboa, Portugal. E-mail: gsoveral@ff.ulisboa.pt*
[c] *Dept. Bioquímica e Biologia Humana, Faculty of Pharmacy, Universidade de Lisboa, 1649-003 Lisboa, Portugal*
[d] *Department of Biochemistry, Groningen Biomolecular Sciences and Biotechnology Institute, University of Groningen, Nijenborgh 4, 9747 AG Groningen, The Netherlands*
[e] *Research Center "Linking Landscape, Environment, Agriculture and Food" (LEAF), Instituto Superior de Agronomia, Universidade de Lisboa, 1349-017 Lisboa, Portugal*
[f] *School of Chemistry, Cardiff University, Main Building, Park Place, Cardiff CF10 3AT, UK. E-mail: casinia@cardiff.ac.uk*

† Electronic supplementary information (ESI) available. See DOI: 10.1039/c6mb00013d

‡ A. de Almeida and A. P. Martins contributed equally to this work.

by glycerol, these differences may be correlated with protein function in different cells and organs.

In general, a better understanding of human aquaglyceroporin regulation in biological environments by different stimuli and the identification of mechanisms of water/glycerol flux modulation may lead to the design of novel inhibitors with potential therapeutic applications. It is worth mentioning that so far only a few molecules have been reported to be AQP inhibitors,[7] and only one family of gold-based compounds has been shown to be selective for aquaglyceroporins.[24–26]

In this context we decided to focus our investigation on AQP3 due to the fact that this isoform has a wide tissue distribution in the epithelial cells of kidneys, airways and skin, suggesting a role in water reabsorption, mucosal secretions, skin hydration, and cell volume regulation.[27] Moreover, recent studies demonstrated an aberrant AQP3 expression in tumour cells of different origins, particularly in aggressive tumours,[28] suggesting this enhanced protein expression to be of diagnostic and prognostic value.

The first publication in 1999, describing AQP3 gating by pH, used *Xenopus* oocytes expressing rat AQP3 (rAQP3) and revealed only a slightly different pK_a for water and glycerol permeability (6.4 and 6.1, respectively) but a markedly different Hill coefficient. In fact, the Hill slope was calculated to be *ca.* 3 for water and 6 for glycerol permeability, respectively.[21] At the time of this first study, little was understood about the possible conformation or residue distribution in the folded functional AQP3, leading the authors to speculate that the pH sensitive residues would be along the channel. Instead, in a later report by Zelenina *et al.*,[22] who studied the mechanism of pH gating of human AQP3 (hAQP3) transfected into lung cells, thanks to the availability of additional sequence information, it could be hypothesized that the pH sensitive residues are likely to be located in loops at the monomers' interfaces, within the AQP3 tetrameric assembly, instead of lining the protein channel. Moreover, four main amino acid residues were identified as pH-sensitive residues by site-directed mutagenesis: His53, His154, Tyr124 and Ser152, all located in extracellular loops. Mutations in these residues led to loss of pH sensitivity, a decrease in water permeability or a shift in the pH sensitivity range.[22] However, in this study the effects of pH gating on permeation by glycerol were not described. Interestingly, both papers postulate that the differences in Hill slope values for water and glycerol are mainly due to different hydrogen bonding capability of the two substrates, while permeating the monomeric aquaporin pore.[21,22] However, so far, this idea remains to be validated.

Thus, we investigated the pH gating of rAQP3, in a different system than previously reported, using this isoform homolog expressed in yeast. Furthermore, we extended our study to human AQP3 and its effects on both water and glycerol permeability using human red blood cells (hRBC), considered a very good model to assess AQP3 activity.[24] Our data show that both human and rat AQP3 are gated by pH, the latter with the pH gating parameters here described for the first time. However, different features were observed for glycerol and water permeation in the two cases. Through molecular modelling studies, we could study the pH dependent closure/opening of the hAQP3 channel at a molecular level, allowing us to predict gating mechanisms of this isoform and possibly of other aquaglyceroporins. The obtained results are discussed in terms of the putative physiological roles of pH gating in aquaglyceroporins and the opening of new possibilities to inhibitor design.

Experimental section

Ethics statement

Venous blood samples were obtained from healthy human volunteers following a protocol approved by the Ethics Committee of the Faculty of Pharmacy of the University of Lisbon. Informed written consent was obtained from all participants.

Strains, plasmids and growth conditions

Plasmid with *Rattus norvegicus* aquaporin-3 (rAQP3) cDNA (pcDNA3-AQP3), kindly provided by Dr M. Eschevarria, Virgen del Rocio University Hospital-Seville, was used for AQP3 cDNA amplification. The centromeric plasmid pUG35 was used for cloning rat AQP3, conferring C-terminal GFP tagging, a MET25 promoter and a CYC1-T terminator.

Escherichia coli DH5α[29] was used as a host for routine propagation of the plasmids. *E. coli* transformants were maintained and grown in Luria-Bertani broth (LB) at 37 °C, 100 μg ml^{-1} of ampicillin.[30] Plasmid DNA from *E. coli* was isolated using a GenElute™ Plasmid Miniprep Kit (Sigma-Aldrich).

Saccharomyces cerevisiae, 10560-6B *MATα leu2::hisG trp1::hisG his3::hisG ura352 aqy1D::KanMX aqy2D::KanMX* (YSH1770, further indicated as *aqy*-null), was used as a host strain for heterologous expression of rat *AQP3*. Yeast strains were grown at 28 °C with orbital shaking in YNB (yeast nitrogen base) without amino acids (DIFCO), with 2% (w/v) glucose supplemented with the adequate requirements for prototrophic growth.[31] Yeast transformants were maintained in the same YNB medium with 2% (w/v) agar. For stopped-flow assays, the same medium was used for yeast cell growth.

Cloning of rAQP3 and yeast transformation

E. coli DH5α was transformed with (pcDNA3_AQP3) and used for propagation of the plasmid. Plasmidic DNA was isolated and purified.

rAQP3 specific primers modified to incorporate restriction sites for SpeI (underlined) and ClaI (underlined) (5′-GGACTAGTCCT ATG GGT CGA CAG AAG GAG TTG AT-3′ and 5′-CCAT CGATGGA GAT CTG CTC CTT GTG CTT CAT GT-3′ respectively) were designed and used for PCR amplification of r*AQP3* cDNA. PCR amplification was carried out in an Eppendorff thermocycler using Taq Change DNA polymerase (NZYTech). The PCR product was digested with SpeI and ClaI restriction enzymes (Roche Diagnostics®), purified using a Wizard® SV Gel and PCR Clean-Up System kit (Promega) and cloned into the corresponding restriction sites of pUG35 digested with the same restriction enzymes, behind the MET25 promoter and in frame with the GFP sequence and CYC1-T terminator, using

T4 DNA Ligase (Roche), according to standard protocols,[30] to construct the expression plasmid pUG35-rAQP3.

The plasmid was used to transform DH5α *E. coli* strain, propagated and subjected to extraction and purification. Fidelity of constructs and correct orientation were verified by PCR amplification, restriction analysis and DNA sequencing. Agarose gel electrophoresis and restriction site mapping were performed according to standard methods.[30,32] Transformation of the *S. cerevisiae aqy*-null strain with pUG35-rAQP3 was performed using the lithium acetate method described in ref. 32. The same strain was also transformed using an empty pUG35 vector (which does not contain rAQP3 cDNA) to be used as a control (further indicated as control). Transformants were selected on YNB medium without uracil as an auxotrofic marker.

rAQP3 subcellular location by fluorescence microscopy

For subcellular localization of GFP-tagged rAQP3 in *S. cerevisiae*, yeast transformants in the mid-exponential phase were observed using a Zeiss Axiovert 200 fluorescence microscope, at 495 nm excitation and 535 nm emission wavelengths. Fluorescence microscopy images were captured using a digital camera (CoolSNAP EZ, Photometrics, USA) and using the Metafluor software (Molecular Devices, Sunyvale, CA).

Cell sampling and preparation

Venous blood samples were collected in a citrate anticoagulant (2.7% citric acid, 4.5% trisodium citrate and 2% glucose). Fresh blood was centrifuged at 750 × *g* for 5 min at 4 °C, and plasma and the buffy coat were discarded. Packed erythrocytes were washed three times in phosphate buffer saline solution (PBS; KCl 2.68 mM, NaCl 137 mM, KH_2PO_4 and Na_2HPO_4 concentration was varied in order to change the pH in the range of 5–7.8 maintaining the total osmolarity constant at 310 mOsM), diluted to 0.5% hematocrit and immediately used for experiments. Yeast transformants were grown up to $OD_{640\,nm} \approx 1$, harvested by centrifugation (5000 × *g*; 10 min; 4 °C), washed and re-suspended in ice-cold sorbitol (1.4 M) K^+-citrate buffer (50 mM, pH 5–7.8) up to a concentration of 0.33 g ml^{-1} wet weight and kept in ice for at least 90 minutes. Prior to the osmotic challenges the cell suspension was pre-loaded with the nonfluorescent precursor 5-and-6-carboxyfluorescein diacetate (CFDA, 1 mM for 10 min at 30 °C) that is cleaved intracellularly by nonspecific esterases and generates the impermeable fluorescent form known to remain in the cytoplasm.[33] Cells were then diluted (1 : 10) in sorbitol 1.4 M buffer and immediately used for experiments.

Cell volume measurements

The equilibrium volume of hRBC in PBS solutions at different pH values was determined using a CASY-1 Cell Counter (Scharfe System GmbH, Reutlingen, Germany) and was calculated to be 86 fL for the experimental pH range used in the permeability assays. Mean volumes of yeast transformants equilibrated in sorbitol 1.4 M buffer were obtained by loading cells with CFDA under a fluorescence microscope equipped with a digital camera as previously described.[33] Cells were assumed to have a spherical shape with a diameter calculated as the average of the maximum and minimum dimensions of each cell.

Stopped-flow experiments

Light scattering and fluorescence stopped-flow spectroscopy was used to monitor cell volume changes of, respectively, RBC[34] and yeast transformants loaded with the concentration-dependent self-quenching CFDA fluorophore.[33] Experiments were performed on a HI-TECH Scientific PQ/SF-53 stopped-flow apparatus, which has a 2 ms dead time, temperature controlled, interfaced with an IBM PC/AT compatible 80386 microcomputer. After challenging cell suspensions with an equal volume of shock solution at 23 °C, the time course of volume change was measured by following the 90° scattered light intensity at 400 nm, or fluorescence intensity (excitation 470 nm and emission 530 nm). For each experimental condition, 5 to 7 replicates were analysed. Baselines were acquired using the respective incubation buffers as isotonic shock solutions.

For osmotic water permeability (P_f) measurements, a hyperosmotic shock solution containing a non-permeable solute was used (for RBC assays, sucrose 200 mM in PBS pH 5 to 7.8; for yeast assays, sorbitol 2.1 M in K^+-citrate pH 5 to 7.8) producing an inwardly directed gradient of the solute.

To measure glycerol permeability (P_{gly}), a hyperosmotic shock solution containing glycerol was used (for RBC assays, glycerol 200 mM in PBS pH 5 to 7.8; for yeast assays, sorbitol 0.7 M, glycerol 1.4 M in K^+-citrate pH 5 to 7.8) creating an inwardly directed glycerol gradient. After the first fast cell shrinkage due to water outflow, glycerol influx in response to its chemical gradient was followed by water influx with subsequent cell re-swelling.

In all the permeability assays the magnitude of the osmotic shocks (given by the ratio of the initial to final medium osmolarity after the applied osmotic challenges) was similar (tonicity of 1.25 to 1.5).

Data analysis

P_f was estimated by $P_f = k\,(V_o/A)(1/V_w(osm_{out}))$, where V_w is the molar volume of water, V_o/A is the initial cell volume to area ratio, (osm_{out}) is the final medium osmolarity after the applied osmotic gradient and k is the single exponential time constant fitted to the light scattering or fluorescence signal of yeast[33] or RBC shrinkage.[34]

For hRBC, P_{gly} was calculated by $P_{gly} = k\,(V_o/A)$, where V_o/A is the initial cell volume to area ratio and k is the single exponential time constant fitted to the light scattering signal of glycerol influx in erythrocytes. For yeast cells, fluorescent glycerol traces obtained were corrected by subtracting the baseline slope that reflects the bleaching of the fluorophore. This was attained by fitting each signal to a double exponential with a slope where the first process corresponds to cell shrinkage due to water outflow, the second process to cell swelling due to glycerol influx, and the slope corresponds to the baseline observed in all glycerol traces. The pattern of fitted slopes was confirmed for each experimental condition using baseline traces obtained with control stain under isotonic conditions.

Statistical analysis

The results were expressed as mean ± SEM of n individual experiments. Statistical analysis between groups was performed using the unpaired t-test. P values < 0.05 were considered statistically significant.

Molecular modelling

The 3D structure of hAQP3 was obtained by homology modelling using the Molecular Operating Environment (MOE 2012.10) (CCG 2012).[35] The choice of a template structure was based on the sequence identity between hAQP3 and the sequence of the AQPs with available resolved structures from human, bacteria and *Plasmodium falciparum*. The isoform showing the highest sequence similarity with hAQP3 is the bacterial isoform Glycerol Facilitator (GlpF), which was then chosen as a template structure to generate a homology model of hAQP3. Three resolved structures for bGlpF, crystallized either with or without glycerol and solved by X-ray diffraction, were retrieved from the Protein Data Bank. Among them, the template was selected that had the best resolution (2.70 Å) without any substrate (pdb 1LDI).[36] The tetrameric form was assembled and the structure was prepared and protonated at pH 7 by using the Amber12EHT force field. 50 intermediate models of AQP3 were generated and averaged to obtain the final homology model. The model obtained was checked for reliable rotamers involving the side chains in the regions of ar/R SF and NPA, by comparison with the available crystal structures of all the other human and microbial AQP isoforms (pdb codes 1H6I, 36D8, 3D9S, 1RC2, 1LD1 and 3C02). The structure was protonated at pH 7 and an energy minimization refinement was performed with fixed Cα atoms.

Results and discussion

pH gating of rat AQP3

In our study we first evaluated rAQP3 gating, in a yeast model, using stopped-flow spectroscopy. Functional aquaporin studies, performed using heterologous expression of aquaporins in an *aqy*-null strain of *Saccharomyces cerevisiae*, have been previously described by our group.[19] This yeast strain expresses also two endogenous aquaglyceroporins, which were not silenced: Fps1 and YFL054c. Fps1 is crucial for yeast osmotic adaptation being inactivated within seconds after a hyper-osmotic shock to ensure intracellular retention and accumulation of glycerol.[37] Thus, under our experimental conditions it remains in a closed state induced by high external osmolarity in the permeability assays. Additionally, YFL054c is not permeated by glycerol under normal conditions or when subjected to hyper or hypo osmotic stress.[38] Moreover, deletion of the two aquaglyceroporins can cause changes in cell membrane content, lead to cell wall stress and increased temperature sensitivity, which could influence the output in our experimental setup.[38] Therefore, we optimized an expression system where only the orthodox aquaporins were silenced.

Yeast cells were transformed with either the empty plasmid (control cells) or the plasmid containing the rat AQP3 gene (mentioned as rAQP3 cells, for clarity). The expression of rAQP3 in the *S. cerevisiae* model was assessed by fluorescence microscopy, using GFP tagging. In transformed cells, rAQP3-GFP is localized at the cellular membrane, while cells with empty plasmid have a homogeneous cytoplasmic distribution (Fig. S1 in the ESI†).

The stopped-flow technique allows volume monitoring of cells subjected to hypo and hyperosmotic stress: when cells are exposed to hyperosmotic shock with impermeant solutes, water outflow induces cell shrinkage. Conversely, when the osmotic shock is provided by a permeable solute as glycerol, cells first shrink due to water outflow and afterwards swell again due to glycerol passage. Thus, water and glycerol permeability are then evaluated according to cell swelling or shrinkage monitored by 90° light scattering, detected by the stopped-flow. In the case of the yeast cell model, the cells are pre-loaded with carboxifluorescein, and the fluorescence intensity reflects volume changes.

At first, in order to evaluate if the observed effect was due to AQP3 being expressed in the yeast cells, both groups of control and rAQP3 were incubated at two different pH values, namely pH 5 and 7. These pH conditions were chosen based on previous literature,[21,22] to have closed (pH 5) and open (pH 7) AQP3.

In Fig. 1 the water and glycerol permeabilities (P_f and P_{gly}, respectively) of control and rAQP3 cells are shown. It is possible to observe that, while control cells have no glycerol permeability, they do show basal water permeability under both tested pH conditions, due to the intrinsic water permeability of the membrane lipid bilayer. Interestingly, from panel C of Fig. 1 it is evident that at pH 5, there is no permeation by glycerol, with a significant increase at pH 7, which clearly demonstrates the closed and open states of rAQP3.

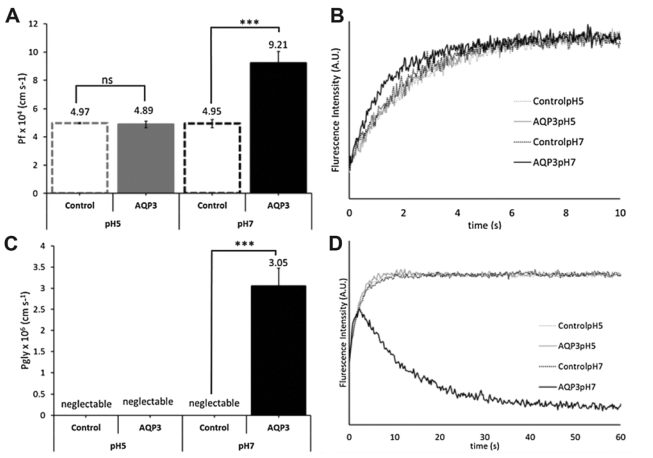

Fig. 1 Water (A and B) and glycerol (C and D) permeability (P_f and P_{gly}) in control yeast cells (transformed with the empty vector) (dashed) and in yeast expressing rAQP3 (solid) at pH 5 (grey) and 7 (black). Panel A shows the water permeability (P_f) of control and AQP3-expressing cells, at pH 5 and pH 7. Panel B shows the changes in fluorescence intensity obtained when yeast transformants are confronted with a hyperosmotic sorbitol solution of tonicity 1.25 triggering cell shrinkage due to water outflow. Panel C shows the glycerol permeability (P_{gly}) of control and AQP3-expressing cells, at pH 5 and pH 7, while panel D shows the changes in fluorescence intensity obtained when cells are confronted with a hyperosmotic glycerol solution. After a first water outflow due to the osmotic gradient, the AQP3-expressing cells re-swell due to glycerol entrance at pH 7. *** $p < 0.001$.

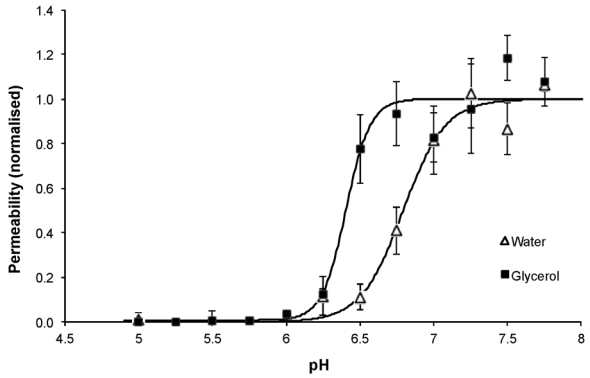

Fig. 2 Water and glycerol permeability (P_f and P_{gly}, normalized) in yeast cells expressing rAQP3 *versus* pH. The fit is according to the Hill equation.

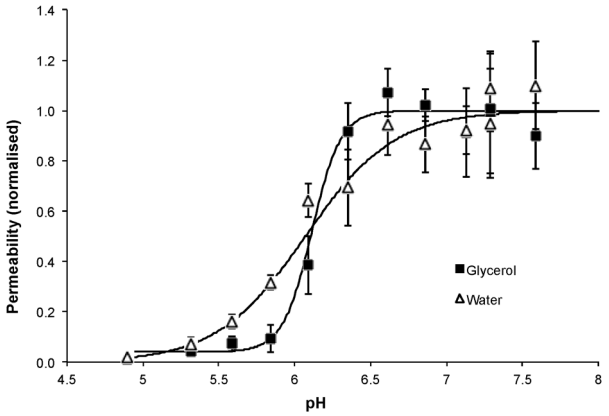

Fig. 3 Water and glycerol permeability (P_f and P_{gly}, normalized) in human red blood cells (hRBC) *versus* pH. The fit is according to the Hill equation.

Table 1 pK_a and Hill slope values for water and glycerol, of human and rat AQP3. Obtained by fitting the data presented in Fig. 2 and 3

	pK_a		Hill slope	
AQP3 variant	Water	Glycerol	Water	Glycerol
Rat	6.80 ± 0.15	6.40 ± 0.20	3.00 ± 0.31	5.30 ± 0.62
Human	6.08 ± 0.01	6.12 ± 0.01	1.64 ± 0.21	3.93 ± 0.91

Since the control cells present a basal water permeability that is not altered by the expression of rAQP3 when incubated at pH 5, it is possible to normalize P_f that corresponds to the permeability of rAQP3 alone. Knowing from these results (Fig. 1) and previous studies that hAQP3 is in a closed state at low pH (*ca.* 5),[21] the normalized water permeability *via* rAQP3 was obtained by subtracting the permeability values of control cells at each pH value. For P_{gly}, this subtraction was not necessary since the control cells show no glycerol permeability at any pH. The rAQP3 permeability for both water and glycerol is shown in Fig. 2. We can observe that the channel is closed for both water and glycerol between pH 5 and 6 and has a maximum permeability at pH 6.5 (glycerol) and pH 7 (water), respectively. This behaviour and Hill slope values found for water and glycerol in the rAQP3 isoform (see Table 1) are similar to those reported previously.[21]

pH gating of human AQP3

Afterwards, we evaluated hAQP3 gating in hRBC. hRBC co-expresses hAQP1 (selective for water) and hAQP3 (permeating water and glycerol) and thus both isoforms contribute for water permeability. Previous studies showed that human AQP1 is not gated by pH,[20,21] and thus any pH-dependent effect on hRBC water permeability would be due to individual gating of hAQP3. Knowing that pH does not influence water permeation *via* a lipid bilayer or *via* hAQP1, water permeability corresponding exclusively to hAQP3 was obtained by subtracting the total cell permeability at pH 5 (where AQP3 is in the closed state[21,22]) from the total permeability at each pH value (Fig. 3).

In accordance with previous studies,[21,22] we observed a maximum permeability for both water and glycerol between pH 6.5 and 7.5, and a decreased permeability and pore closure at lower pH, with the pore completely closed at pH 5.

The calculated pK_a values for both water and glycerol were found to be approximately the same, *ca.* 6.1, with Hill slopes of about 2 and 4, respectively. While the pK_a of glycerol permeability is in accordance with our data for rAQP3, the pK_a value of water is slightly lower (6.1 *vs.* 6.8). Notably, while the Hill coefficients vary from those calculated for rAQP3 – which may be due to both differences in the protein sequence or in the selected cellular model – they have the same 2-fold difference (Table 1). It is worth mentioning that in spite of the strong sequence homology (*ca.* 95%) between the two isoforms (see Fig. S3 in the ESI†) still the 5% difference in sequence may account for a different mechanism of inhibition, as will be discussed further.

Hill coefficients, as black box parameters, may be subjected to different interpretations. One explanation found in the literature for this difference of half the value for water, when compared to glycerol, is based on the Eyring energy barrier model,[39] and explained by the differences in activation energy (E_a) of both solutes. Interestingly, the measured activation energies for water and glycerol in hRBC evidenced a two-fold value for glycerol permeability.[34] It was hypothesized that as E_a for water permeability is low, water molecules cross the channel by forming a single line of hydrogen bonds, while glycerol, with a higher E_a, and having three OH groups, will establish more hydrogen bonds than water molecules when passing through the channel.[39] In fact, such a hydrogen bond network for both water and glycerol is evidenced by X-ray studies of the bacterial glycerol facilitator (bGlpF) channel[40] and of the *P. falciparum* isoform (pfAQP)[41] (Fig. 4). Moreover, glycerol molecules have their OH groups pointing towards the hydrophilic side of the channel, favouring such a hydrogen bond network. In the case of hAQP3, we can also observe this phenomenon in molecular dynamics (MD) simulations.[42] Remarkably, in the latter study the number of hydrogen bonds in the crystal structures, as well as in the MD simulations, is similar to the Hill slopes found by us for hAQP3 in hRBC, approximately 1.5 for water and 4 for glycerol.

Although the importance of H-bonding interactions between substrates and amino acid residues inside the AQP3 channel cannot be underestimated, and certainly plays a role in determining

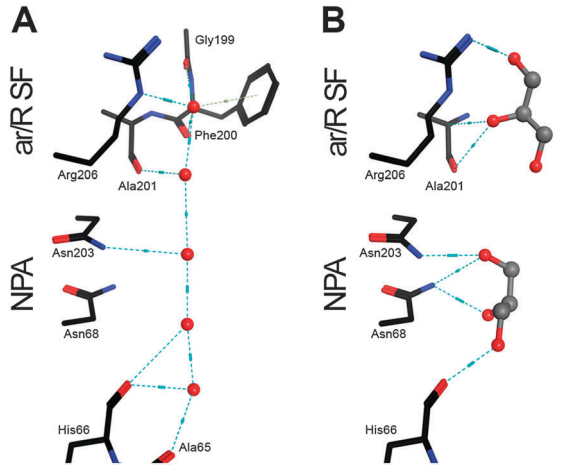

Fig. 4 H-bond network of water (A) and glycerol (B), X-ray structure of bacterial glycerol facilitator (bGlpF) with water (A), pdb1LDA, and glycerol (B), pdb1FX8.

the activation energies of each substrate, recent experimental findings from our groups on the pH gating of aquaglyceroporin-7 (hAQP7) (unpublished data) indicate that the Hill slope is similar for water and glycerol. Therefore, other factors may influence the overall pH gating mechanisms of AQPs, in addition to the number of H-bonds between substrates and the protein channel.

A second explanation for the observed difference in Hill coefficient values is the amount of titrable residues inside the channel, as postulated previously by Zeuthen *et al.*[21] This theory is based on the possible competition between the H^+ and glycerol molecules for the protonable side-chains. A phenomenon of non-competitive inhibition of glycerol binding, by two protons, has been observed in hRBC.[43] The limitation of this theory is the fact that the titrable residues would be located in the channel lining, where they could affect glycerol H-bond formation. Later work on aquaporin sequencing and structure showed that hydrophilic and hydrophobic sides constitute the aquaporin lining and few to no residues are actually titrable.

Interestingly, analysing not only the Hill slope but also the raw data of the titration curve (shown in Fig. 3) the decrease in water permeability appears to have an earlier onset, but also seems to be more gradual than that of glycerol as a function of pH. However, it is important to distinguish between the steepness of the titration curves (Hill slope), which is related to how abruptly the channel stops permeating a substrate, and the exact pH at which we observe a change in permeability. Regarding the different steepness of water and glycerol permeability, the phenomenon may be explained by the smaller size of a water molecule, when compared to glycerol. In fact, protonation of certain residues in the protein, even in loops, may cause structural changes in hAQP3, as seen in other aquaporins,[12,18,44,45] which lead to channel's closure. Such changes may abruptly hinder the passage of a bulkier glycerol molecule at a pH where some water molecules can still flow through. This hypothesis is in line with our studies on aquaporin inhibition by Hg^{2+}, where we described the closure of hAQP3 for glycerol passage, but not for water passage, upon structural changes caused by metal binding.[42]

Based on these considerations, we suggest that the different protonation states of hAQP3 correspond to different structural conformations. Moreover, since the activation energies of water and glycerol have a two-fold difference, higher for glycerol, it suggests that glycerol permeation is much slower. In fact, in our studies on Hg^{2+} inhibition of hAQP3, we observed an unbiased passage of a glycerol molecule and its permeation was much slower than that observed for water.[42] This difference is mainly due to the formation of a higher number of hydrogen bonds inside the channel with lining residues by glycerol.

Investigation of the pH gating mechanism of hAQP3 by molecular modelling

In order to investigate the molecular mechanism of pH gating of hAQP3, a molecular modelling approach previously developed by our group was used.[46] However, in the case of the present study, a homology model of human AQP3 in the tetrameric form was built, instead of the monomeric form, based on the available structure of the bacterial glycerol facilitator (GlpF, pdb code 1LDI).[47] The final model was obtained by averaging 50 individual models, using MOE software (MOE 2012.10; CCG 2012),[35] as described in the Experimental section.

Analysis of the model shows the common fold, shared by the aquaporin family, containing six transmembrane helices and two half-helices, for each monomer. The two half-helices are located inside of the pore of each monomer and contain the typical NPA (Asp-Pro-Ala) motif that constitutes one of the aquaporin's selectivity filters. The residues in these two NPA motifs are Asn83-Pro84-Ala85, and Asn215-Pro216-Ala217 (Fig. S2 in the ESI†). Another selectivity filter, the narrowest part of the channel lining, is located near the extracellular entrance and is named ar/R SF (aromatic/arginine selectivity filter). This selectivity filter is an important structural feature of aquaporins, where the arginine is fully conserved in all mammalian aquaporins (Fig. S2, ESI†). The ar/R SF also serves as a distinctive feature among aquaporins, as the composition in aminoacids may vary in water and glycerol channels: classical aquaporins have an ar/R SF formed by 4 residues, including commonly a phenylalanine and histidine, while aquaglyceroporins' ar/R SF comprises only three residues. Thus, these differences account for pore size and selectivity among aquaporin isoforms. All these features are observed in our model of hAQP3, where Phe63, Tyr212 and Arg218 constitute the ar/R SF (Fig. S2, ESI†).

According to the previously reported site-directed mutagenesis studies, the molecular mechanism behind the gating of AQP3 involves four titrable residues, namely **His53**, **Tyr124**, **Ser152** and **His154**.[22] However, the lack of structural information about this isoform led the authors only to speculate on the type of interactions these residues could possibly establish with unknown surrounding residues, based on possible similar behaviours of histidines, tyrosines and serines in enzymes. Using our homology model of the tetrameric form of hAQP3, it is possible to locate the pointed residues at the interface of the monomers, closer to the extracellular side of the protein (Fig. 5). These residues may be involved in important monomer–monomer interactions and their protonation/deprotonation may affect

the overall assembly of the tetramer and, consequently, of the water and glycerol permeability. In detail, at pH 7 in our model **His53** is located at the central pore lining and its side-chain appears to have the possibility to form H-bonds with residues Thr58, Thr52 and Gln45 in the same monomer while interacting also with the aromatic ring of Phe56, located in an adjacent monomer. These interactions are different in each monomer. Interestingly, mimicking the protonation state of the protein at pH 5 leads to the formation of new H-bonds, namely a second H-bond with Thr52 (this time with its side-chain) Thr204, Gly51 and Thr62. The formation of new H-bonds may cause loop A to move closer to the monomer pore and cause structural modifications in transmembrane-helix 5 (TM5).

On the other hand, **Tyr124** does not appear to have a clear role or to be particularly sensitive to pH changes. Due to its very high pK_a (typical range for a Tyr side-chain in proteins is 9–12[48]), it is unlikely that its side-chain is affected by changes in the pH range from 5 to 8. In addition, the side-chain of Tyr124 appears to be pointing out in the direction of the membrane, not participating in any interaction with other residues. The only apparent interactions of this residue are between its backbone and the backbones of Trp128 and Phe120, contributing to the maintenance of the helical structure. Interestingly, at pH 5, in one monomer it is possible to see the formation of a new H-bond with the backbone of Ile127. This cannot explain the influence of pH on Tyr124 and the possible changes it may induce.

Regarding **Ser152** and **His154**, these residues are located in the region between two adjacent monomers. At pH 7, while the backbone of His154 forms a H-bond with the backbone of Ser152, located in the same loop (loop C), the His154 side-chain forms a H-bond with the side-chain of His129, at the opposite end of loop C of another monomer (Fig. 5B).

At lower pH, the same interactions appear to be maintained and a new H-bond may be formed with the backbone of Gly153. The formation of this new bond in the same loop may weaken the interaction between the two histidines, leading to a movement of loop C towards the channel opening. This disruption, together with the above-described movement of loop A due to

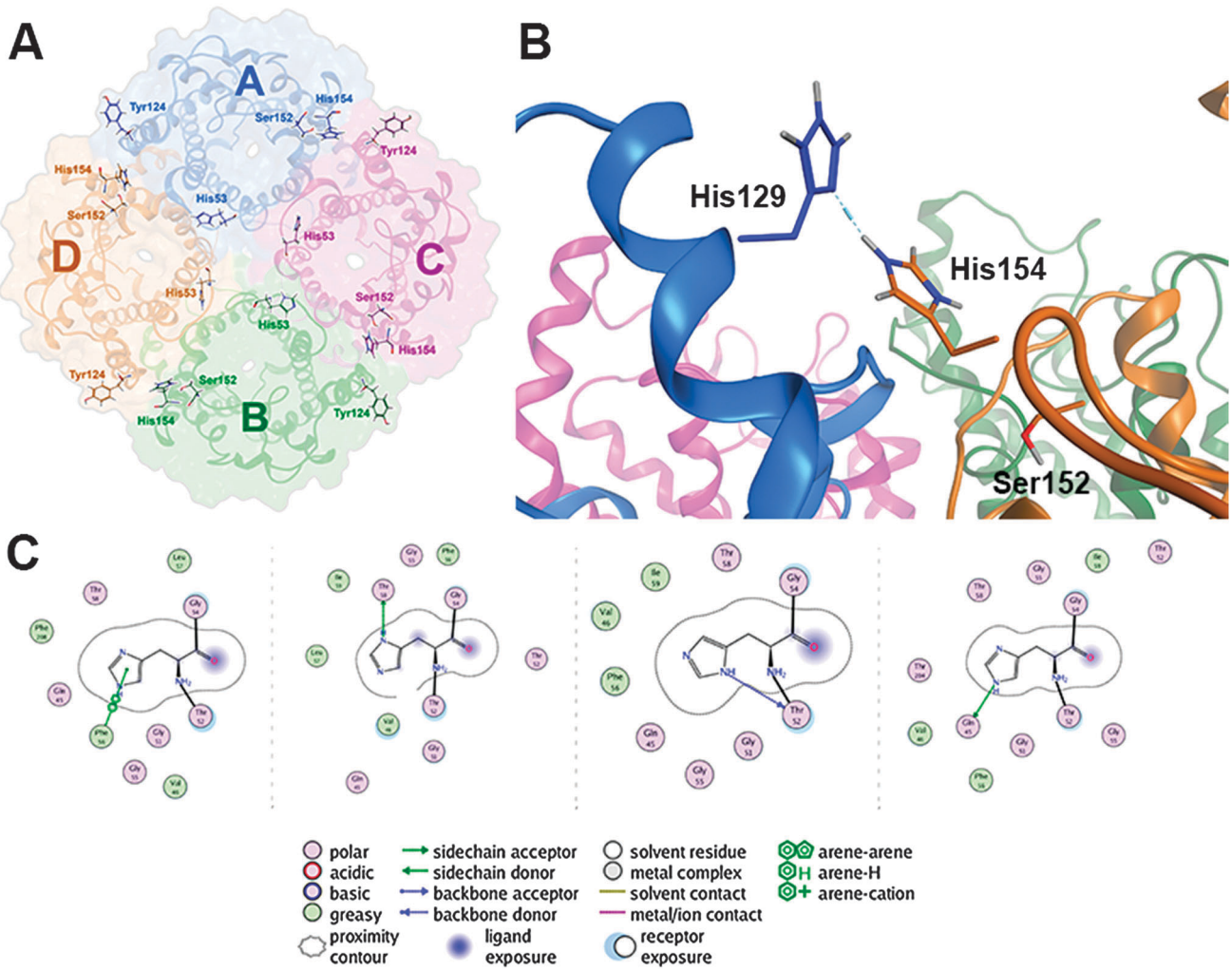

Fig. 5 Homology model of tetrameric human AQP3. (A) Extracellular top view of the tetrameric form of hAQP3 and the position of residues involved in pH regulation. (B) Positions of His129 from monomer A and His154 from monomer D, as well as Ser152. The dashed blue line represents the H-bond formed between the two histidines at pH 7. (C) Scheme of the interactions of His154 with neighbouring residues, at pH 7, for each of the 4 monomers.

protonation of His53, may be the cause for blockage of the channel for water and glycerol permeability. This structural change of movement of loop C was also observed in the MD studies on mercury inhibition of hAQP3, which leads to a collapse of the ar/R SF.[42] This movement may not be simultaneous as, due to neighbouring amino acid side-chains, the pK_a of His53 and His154 may be subjected to small variation, causing a gradual conformational change with a pH decrease (or increase).

Previous studies by Zelenina *et al.* show that a mutation of His129 to an alanine residue does not affect water permeability or change the pH sensitivity range.[22] However, glycerol permeability was not measured and the contribution of this residue to the mechanism of inhibition of hAQP3 by pH, regarding glycerol permeability, cannot be excluded.

Interestingly, loop movement upon pH changes was also observed for the orthodox water channel bovine AQP0 (bAQP0). This isoform has a maximum of permeability similar to that of hAQP3 at pH 6.5; however it is closed at pH 8.5.[49] The residues responsible for pH sensibility were identified by site-directed mutagenesis as two histidines: His40 and His122, in loops A and C, respectively. While His40 in bAQP0 is in a similar position to His53 in our model of hAQP3, His122 is in the position corresponding to Ser152 (and close to His154) in hAQP3 (Fig. S4 in the ESI†). Overall, as described for bAQP0, we propose that key histidines in loops A and C that span the outer vestibule contribute to pH sensitivity in hAQP3. Moreover, insertion of two histidines in similar positions in hAQP1, a non pH-gated aquaporin, induced pH sensitivity in the same range as bAQP0,[49] further confirming the key role of these residues in pH gating.

As observed for the MD study on Hg^{2+} inhibition of hAQP3, by Spinello *et al.*,[42] the closed state of bAQP0 involves the movement of a loop (in this case loop A) and a collapse of the ar/R SF (Fig. S5 in the ESI†), shown in the X-ray structures of the open and closed bAQP0.[50] This collapse in the SF appears to be different from the one described for hAQP3, most likely due to differences in amino acid composition and diameter of the channel. Mutations in the histidine of loop A – His40 in AQP0[49] and His53 in AQP3[22] – showed a shift of the pH sensitivity towards a more alkaline range. This effect supports the idea that the pK_a of histidine residues in different regions of the same protein may be very different, leading to different levels of channel regulation.

Other studies reported that the orthodox water channel AQP4 also shows pH-sensitivity, which was recently attributed to one particular histidine residue, His95, predicted by *in silico* methodologies.[51] His95, located inside the channel and facing the intracellular side, is conserved in all aquaporins, including those that do not show pH-sensitivity, such as AQP1. Therefore, it is difficult to conclude that it is the only one responsible for the observed pH gating mechanism.

rAQP3 *versus* hAQP3

Molecular modelling was useful also to explain observed differences among the Hill slope values of hAQP3 with respect to rAQP3 (see Table 1). Human AQP3 shares a sequence identity higher than 80% with most mammalian AQP3 isoforms. Nonetheless, changes in key residues may change permeability and regulatory features. When compared human and rat AQP3 isoforms, although a sequence similarity of about 95% is observed, they do not share one of the residues that may be involved in the pH gating of the hAQP3, namely His129, which is substituted by an alanine (Fig. S3 in the ESI†). Even though this mutation does not seem to affect water permeability of hAQP3,[22] its effect on glycerol permeability is unknown. Moreover, a mutation of the same residue on a human and rat isoform may not have the same effect, as a network of hydrogen bonds is a very delicate system and is highly dependent on the neighbouring residues. Therefore, we can only conclude that the mutation H129A is able to produce a functional rAQP3 glycerol and water channel. Additionally, it is possible that the differences in the observed pK_a and Hill slope for the human and rat isoforms are due to species differences, even though we cannot exclude the possibility of cell-model differences.

Conclusions

In the present study we investigated the pH gating of rat and human AQP3 by stopped flow spectroscopy. For the first time we were able to fully characterize not only the effects of pH gating on water, but also on glycerol permeability in this human isoform. In the case of water, the obtained results confirm the previous observations of hAQP3 gating in oocytes.[21]

Interestingly, previous reports on rAQP3 pH gating were confirmed in our yeast model, which highlighted differences with the human isoform. In fact, while hAQP3 shows the same pK_a for both water and glycerol, the pK_a values are similar for water, but different for glycerol in the rAQP3 system. These differences may be due to species differences, even though we cannot exclude that the selected investigational system itself may partly lead to this variation.

In the light of the experimental Hill slope values for water and glycerol, a few theories on differences in the pH gating mechanisms of aquaporin permeation have been postulated. Current knowledge about the aquaporin sequence and structure allows us to discard the hypothesis of protonation of residues inside the channel.

Previous mutagenesis studies highlighted four key residues -- His53, Tyr124, Ser152 and His154 – in hAQP3 pH gating and their effects on water permeability, but could not give a comprehensive analysis of the role of these residues.[22] Based on our experimental data (pK_a and the Hill slope of hAQP3), and using a tetrameric homology model of hAQP3, we investigated the AQP3 gating mechanisms at a molecular level, disclosing the interactions of the four key amino acidic residues in the context of the functional aquaporin quaternary-structure. Specifically, we can now conclude the following:

(i) The four key amino acids are located in extracellular loops (A and C) in each hAQP3 monomer.

(ii) Protonation of pH-sensitive residues of hAQP3 may not occur simultaneously, but gradually, causing progressive structural changes as a function of pH.

(iii) Movement of loop C in the outer vestibule of hAQP3, as observed previously in MD studies,[42] may cause a blockage of the larger glycerol molecule, while still allowing the permeation of water. A similar movement may occur in loop A.

(iv) hAQP3 monomers may not behave in a concerted fashion, but rather independently, and fluxes of solutes may be different in each monomer, upon pH changes. The observable effect of pH on AQP3 permeation is a sum of the effects in all the four monomers and, as a consequence, our observation of the differences in the Hill slope for water and glycerol may not be the same for each independent monomer, but an ''average'' effect of the tetrameric assembly.

Overall, *in silico* methodologies have allowed us and others[12,51] to perform a detailed molecular analysis of the gating mechanism of AQPs, providing a more physiological view of such processes. Moreover, the movement of loops, intra or extracellular, was observed in the gating mechanism of several AQPs[12,18,44,45] and appears to be a crucial feature in channel closure. Histidine residues in such loops can ''tune'' the pH sensitivity towards certain pH values.[22,49]

Notably, metal compounds have also been shown to modulate the function of AQPs. For example, among the endogenous transition metal ions, Cu^{2+} and Ni^{2+} have been demonstrated to cause a decrease in water and glycerol permeability (P_f and P_{gly}) in cells expressing human AQP3-GFP in a dose-dependent manner and the effect was rapid and reversible, while Pb^{2+} and Zn^{2+} ions had no effect in AQP3 permeability.[22,23]

Moreover, the effect of Ni^{2+} was pH-dependent: at neutral and acidic pH, the AQP3-mediated water permeability was completely inhibited by 1 mM $NiCl_2$. At pH 7.4 and 8.0, the P_f in transfected cells was decreased by Ni^{2+}, but remained significantly higher than that in non-transfected cells. Site-directed mutagenesis studies identified three residues, Trp128 and Ser152 in the second extracellular loop and His241 in the third extracellular loop of AQP3, as determinants of Ni^{2+} inhibition effects.[22] These Ni^{2+}-sensitive residues are the same as for Cu^{2+}, which suggests the same binding site and mechanism of inhibition.[23] Interestingly, Ser152 was identified as a common determinant of both Ni^{2+} and pH sensitivity.

These findings confirm our idea that knowledge of the physiological mechanisms of AQP gating may open the way to new strategies to selectively target different AQPs and to achieve optimization of inhibitors, such as the recently reported gold-based compounds[24,26,52] potentially active also as His binders. Finally, considering the importance of glycerol in multiple vital physiological processes, regulation of its permeation across hydrophobic cell membranes *via* AQPs may be crucial for cell proliferation, adaptation and survival, and future research to untangle the biological relevance of aquaglyceroporins' pH gating in health and disease conditions ought to be conducted.

Acknowledgements

EU COST Action CM1106 is acknowledged for financial support.

Notes and references

1 in *Aquaporins in health and disease: new molecular targets for drug discovery*, ed. G. Soveral, S. Nielsen and A. Casini, CRC Press, Taylor & Francis Group, Boca Raton, FL, 2016.
2 G. Benga, *Mol. Aspects Med.*, 2012, **33**, 514–517.
3 M. Yasui, A. Hazama, T.-H. Kwon, S. Nielsen, W. B. Guggino and P. Agre, *Nature*, 1999, **402**, 184–187.
4 L. R. Soria, E. Fanelli, N. Altamura, M. Svelto, R. A. Marinelli and G. Calamita, *Biochem. Biophys. Res. Commun.*, 2010, **393**, 217–221.
5 A. Almasalmeh, D. Krenc, B. Wu and E. Beitz, *FEBS J.*, 2014, **281**, 647–656.
6 A. Madeira, S. Fernandez-Veledo, M. Camps, A. Zorzano, T. F. Moura, V. Ceperuelo-Mallafre, J. Vendrell and G. Soveral, *Obesity*, 2014, **22**, 2010–2017.
7 A. S. Verkman, M. O. Anderson and M. C. Papadopoulos, *Nat. Rev. Drug Discovery*, 2014, **13**, 259–277.
8 L. Méndez-Giménez, A. Rodríguez, I. Balaguer and G. Frühbeck, *Mol. Cell. Endocrinol.*, 2014, **397**, 78–92.
9 K. Kalman, K. L. Nemeth-Cahalan, A. Froger and J. E. Hall, *J. Biol. Chem.*, 2008, **283**, 21278–21283.
10 G. Fischer, U. Kosinska-Eriksson, C. Aponte-Santamaria, M. Palmgren, C. Geijer, K. Hedfalk, S. Hohmann, B. L. de Groot, R. Neutze and K. Lindkvist-Petersson, *PLoS Biol.*, 2009, **7**, e1000130.
11 S. Törnroth-Horsefield, K. Hedfalk, G. Fischer, K. Lindkvist-Petersson and R. Neutze, *FEBS Lett.*, 2010, **584**, 2580–2588.
12 L. Janosi and M. Ceccarelli, *PLoS One*, 2013, **8**, e59897.
13 G. Soveral, A. Madeira, M. C. Loureiro-Dias and T. F. Moura, *Biochim. Biophys. Acta*, 2008, **1778**, 2573–2579.
14 M. Ozu, R. A. Dorr, F. Gutierrez, M. T. Politi and R. Toriano, *Biophys. J.*, 2013, **104**, 85–95.
15 L. Leitao, C. Prista, M. C. Loureiro-Dias, T. F. Moura and G. Soveral, *Biochem. Biophys. Res. Commun.*, 2014, **450**, 289–294.
16 L. Verdoucq, A. Grondin and C. Maurel, *Biochem. J.*, 2008, **415**, 409–416.
17 K. L. Nemeth-Cahalan and J. E. Hall, *J. Biol. Chem.*, 2000, **275**, 6777–6782.
18 C. Tournaire-Roux, M. Sutka, H. Javot, E. Gout, P. Gerbeau, D.-T. Luu, R. Bligny and C. Maurel, *Nature*, 2003, **425**, 393–397.
19 L. Leitão, C. Prista, T. F. Moura, M. C. Loureiro-Dias and G. Soveral, *PLoS One*, 2012, **7**, e33219.
20 K. L. Nemeth-Cahalan and J. E. Hall, *J. Biol. Chem.*, 2000, **275**, 6777–6782.
21 T. Zeuthen and D. a. Klaerke, *J. Biol. Chem.*, 1999, **274**, 21631–21636.
22 M. Zelenina, A. a. Bondar, S. Zelenin and A. Aperia, *J. Biol. Chem.*, 2003, **278**, 30037–30043.
23 M. Zelenina, S. Tritto, A. a. Bondar, S. Zelenin and A. Aperia, *J. Biol. Chem.*, 2004, **279**, 51939–51943.
24 A. P. Martins, A. Marrone, A. Ciancetta, A. Galán Cobo, M. Echevarría, T. F. Moura, N. Re, A. Casini and G. Soveral, *PLoS One*, 2012, **7**, e37435.

25 A. Madeira, A. de Almeida, C. de Graaf, M. Camps, A. Zorzano, T. F. Moura, A. Casini and G. Soveral, *ChemBioChem*, 2014, **15**, 1487–1494.
26 A. P. Martins, A. Ciancetta, A. de Almeida, A. Marrone, N. Re, G. Soveral and A. Casini, *ChemMedChem*, 2013, **8**, 1086–1092.
27 M. Hara and A. S. Verkman, *Proc. Natl. Acad. Sci. U. S. A.*, 2003, **100**, 7360–7365.
28 A. de Almeida, G. Soveral and A. Casini, *MedChemComm*, 2014, **5**, 1444–1453.
29 D. Hanahan, in *DNA cloning: a practical approach*, ed. D. M. Glover, IRL Press, Oxford, United Kingdom, 1985, vol. 1, pp. 109–135.
30 E. F. F. J. Sambrook and T. Maniatis, *Molecular Cloning: A Laboratory Manual*, Cold Spring Harbor, NY, 2nd edn, 1989.
31 J. T. Pronk, *Appl. Environ. Microbiol.*, 2002, **68**, 2095–2100.
32 R. D. Gietz and R. H. Schiestl, *Methods Mol. Cell. Biol.*, 1995, **5**, 255–269.
33 G. Soveral, A. Madeira, M. C. Loureiro-Dias and T. F. Moura, *Appl. Environ. Microbiol.*, 2007, **73**, 2341–2343.
34 E. Campos, T. F. Moura, A. Oliva, P. Leandro and G. Soveral, *Biochem. Biophys. Res. Commun.*, 2011, **408**, 477–481.
35 M. O. E. (MOE), Chemical Computing Group Inc. Montreal, QC, Canada, **2012.10**.
36 D. Fu, A. Libson, L. J. W. Miercke, C. Weitzman, P. Nollert, J. Krucinski and R. M. Stroud, *Science*, 2000, **290**, 481–486.
37 M. J. Tamas, K. Luyten, F. C. Sutherland, A. Hernandez, J. Albertyn, H. Valadi, H. Li, B. A. Prior, S. G. Kilian, J. Ramos, L. Gustafsson, J. M. Thevelein and S. Hohmann, *Mol. Microbiol.*, 1999, **31**, 1087–1104.
38 D. Ahmadpour, C. Geijer, M. J. Tamas, K. Lindkvist-Petersson and S. Hohmann, *Biochim. Biophys. Acta*, 2014, **1840**, 1482–1491.
39 J. Nieto-Frausto and B. Kleutsch, *Biochim. Biophys. Acta*, 1992, **1111**, 81–92.
40 D. Fu, A. Libson and R. Stroud, *Novartis Found Symp.*, 2002, **245**, 51–61.
41 Z. E. R. Newby, J. O'Connell Iii, Y. Robles-Colmenares, S. Khademi, L. J. Miercke and R. M. Stroud, *Nat. Struct. Mol. Biol.*, 2008, **15**, 619–625.
42 A. Spinello, A. de Almeida, A. Casini and G. Barone, *J. Inorg. Biochem.*, 2015, DOI: 10.1016/j.jinorgbio.2015.11.027.
43 W. D. Stein, *Biochim. Biophys. Acta*, 1962, **59**, 47–65.
44 A. Frick, M. Järvå and S. Törnroth-horsefield, *FEBS Lett.*, 2013, **587**, 989–993.
45 S. Törnroth-Horsefield, Y. Wang, K. Hedfalk, U. Johanson, M. Karlsson, E. Tajkhorshid, R. Neutze and P. Kjellbom, *Nature*, 2006, **439**, 688–694.
46 A. Madeira, M. Camps, A. Zorzano, T. F. Moura and G. Soveral, *PLoS One*, 2013, **8**, e83442.
47 E. Tajkhorshid, P. Nollert, M. O. Jensen, L. J. Miercke, J. O'Connell, R. M. Stroud and K. Schulten, *Science*, 2002, **296**, 525–530.
48 D. G. Herries, *Biochem. Educ.*, 1985, **13**, 146.
49 K. L. Németh-Cahalan, K. Kalman and J. E. Hall, *J. Gen. Physiol.*, 2004, **123**, 573–580.
50 T. Gonen, Y. Cheng, P. Sliz, Y. Hiroaki, Y. Fujiyoshi, S. C. Harrison and T. Walz, *Nature*, 2005, **438**, 633–638.
51 S. Kaptan, M. Assentoft, H. P. Schneider, R. A. Fenton, J. W. Deitmer, N. MacAulay and B. L. de Groot, *Structure*, 2015, **23**, 2309–2318.
52 A. Serna, A. Galan-Cobo, C. Rodrigues, I. Sanchez-Gomar, J. J. Toledo-Aral, T. F. Moura, A. Casini, G. Soveral and M. Echevarria, *J. Cell. Physiol.*, 2014, **229**, 1787–1801.